

## ARTICLE OPEN

## Displacement Current in Domain Walls of Bismuth Ferrite

Sergey Prosandeev<sup>1,2</sup>, Yurong Yang<sup>1</sup>, Charles Paillard<sup>1</sup> and L. Bellaiche<sup>1</sup>

In 1861, Maxwell conceived the idea of the displacement current, which then made laws of electrodynamics more complete and also resulted in the realization of devices exploiting such displacement current. Interestingly, it is presently unknown if such displacement current can result in large intrinsic ac current in ferroic systems possessing domains, despite the flurry of recent activities that have been devoted to domains and their corresponding conductivity in these compounds. Here, we report first-principles-based atomistic simulations that predict that the transverse (polarization-related) displacement currents of 71° and 109° domains in the prototypical BiFeO<sub>3</sub> multiferroic material are significant at the walls of such domains and in the GHz regime, and, in fact, result in currents that are at least of the same order of magnitude than previously reported dc currents (that are likely extrinsic in nature and due to electrons). Such large, localized and intrinsic ac currents are found to originate from low-frequency vibrations at the domain walls, and may open the door to the design of novel devices functioning in the GHz or THz range and in which currents would be confined within the domain wall.

npj Computational Materials (2018)4:8; doi:10.1038/s41524-018-0066-y

## INTRODUCTION

Domain walls in ferroic materials have attracted a lot of interest because they exhibit enhanced or potentially new properties,<sup>1</sup> such as high conductivity<sup>2–5</sup> or even low-temperature superconductivity,<sup>6</sup> as compared to the heart of domains or to bulks. They also exhibit new functionalities, and may serve as nanoscale chemical reactors<sup>7</sup> or as information carriers in racetrack memory architectures.<sup>8</sup> Such walls are interfaces bridging two domains with different orientation of the ferroic order parameter, for instance domains of alternating polarization. For example and because of the rhombohedral symmetry of its R3c ground state, three types of neutral domain walls (DWs) can occur in the intensively investigated BiFeO<sub>3</sub> (BFO) multiferroic system (inside which polarization and magnetic ordering coexist at room temperature): 71°, 109° and 180° domains, each denoting the angle between the polarization directions on each side of the wall. Such domains were characterized using modern nanoscale techniques such as piezoforce microscopy.<sup>9,10</sup> Interestingly, it was observed that several of those domain walls exhibit larger static conductivity than their adjacent domains by one or more orders of magnitude, even if the domain wall is globally neutral.<sup>2–4,11–13</sup> The origin of the increase in conductivity of the domain wall remains however disputed. Among possible cause, the flexoelectric and potential deformation effects have been invoked to result in band bending at the domain wall, subsequently resulting in local accumulation of free carriers at the DW.<sup>14</sup> A similar idea of local band-gap reduction at the DW was put forward in ref. <sup>15</sup>, but revoked in latter ab initio studies.<sup>16,17</sup> Many works have also considered that defects would play an important role in the enhanced conductivity of DWs.<sup>3</sup> Indeed, it was recently revealed that charged defects accumulate at DWs in BFO,<sup>18</sup> giving further proofs in favor of an extrinsic nature of the conductivity of neutral domain walls. As a result, conductivity of DWs may be

extremely dependent on the synthesis and processing steps, as demonstrated by the loss of conductivity of BFO samples prepared in oxygen-rich atmosphere,<sup>3</sup> which may render the application of conductive DWs difficult at an industrial scale. Rather, finding, understanding and eventually being able to tailor an *intrinsic* mechanism of conduction in DWs would be extremely beneficial towards their large-scale application.

Moreover, two recent studies investigated the ac conductivity of some oxides,<sup>19,20</sup> by employing a scanning microwave impedance microscope. Both of these studies found a strong increase of the conductivity at microwave frequencies, as compared to dc conductivity. Note that the nature of this conductivity can be different, as discussed in refs. <sup>19,20</sup>. In particular, Tselev et al.<sup>19</sup> mostly considered defect-related ac conductivity. On the other hand, ref. <sup>20</sup> discusses the possibility of bound-charge oscillation rather than free-carrier conduction. Such possibility is physically plausible since displacement currents, caused by the oscillatory motion of bound polarization charges under an oscillating electric field, have the potential to lead to an intrinsic mechanism of conduction, i.e., not related to defects a priori.<sup>21</sup> In our minds, there are questions related to displacement currents that need to be addressed. First of all, is the domain wall a better conductor than the domains under an ac exciting field? Secondly, how does it compare to currents of electronic origin, whose magnitude can in a first approximation be taken as that of the dc current reported in experiments? Answering those questions in BFO, by means of an atomistic effective Hamiltonian approach,<sup>22–25</sup> is the main focus of this article. In a first time, it will be shown that displacement currents are indeed larger at the DW than inside the domains. Secondly, an original layer-by-layer decomposition of the dielectric response will demonstrate that the DW exhibits extra-modes of excitation as compared to the bulk, therefore providing new excitation channels. We also compare the

<sup>1</sup>Physics Department and Institute for Nanoscience and Engineering, University of Arkansas, Fayetteville, AR 72701, USA and <sup>2</sup>Institute of Physics and Physics Department of Southern, Federal University, Rostov-na-Donu 344090, Russia

Correspondence: Sergey Prosandeev (sprossan@uark.edu) or Yurong Yang (yurwater@uark.edu)

Received: 25 October 2017 Revised: 2 February 2018 Accepted: 11 February 2018

Published online: 08 March 2018

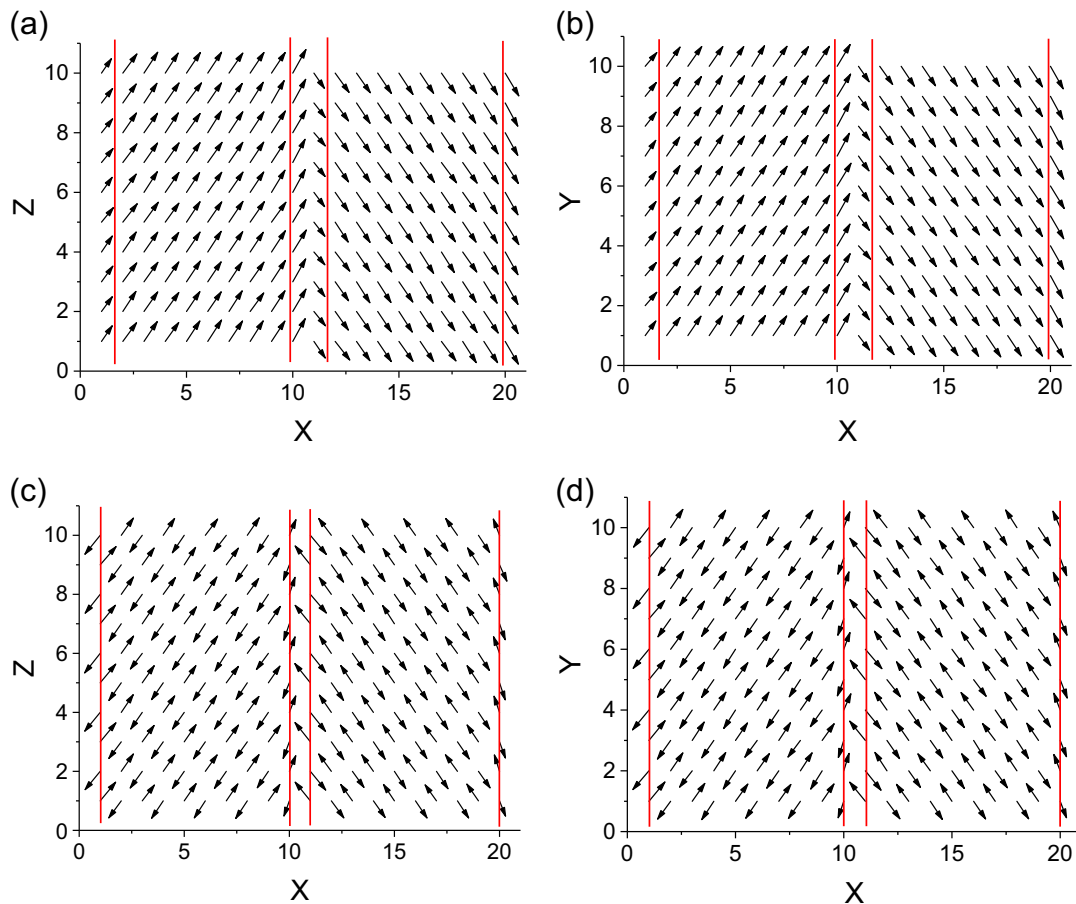


**Fig. 1** Snapshots of the electric dipoles (**a, b**) and AFD patterns (**c, d**) in our  $109^\circ$  domain, as calculated in the present study for a time  $t = 500$  ps and an  $ac$  electric field of  $0.2 \sqrt{3}10^8$  V/m magnitude and 2.5 GHz frequency applied along the pseudo-cubic [111] direction. The red solid lines show the positions of the domain walls. Only a given (010) plane and a (001) plane are shown here

displacement current to dc currents reported in the literature, and predict that displacement currents can be a sizable contribution to the total current in the GHz and THz ranges, which may therefore be put in use to design original devices operating in these frequencies.

## RESULTS

### Effective Hamiltonian

We employ here the effective Hamiltonian method developed in ref. <sup>26</sup> within Molecular Dynamics (MD) technique,<sup>27,28</sup> in order to investigate dynamics of domain walls in BiFeO<sub>3</sub> bulks being under  $ac$  electric fields. Technically, this effective Hamiltonian includes the following degrees of freedom: (1) the local modes  $u_i$  in each 5-atom unit cell  $i$  that are centered on the Bi sites and that are proportional to the electric dipole moment of this cell; (2) the homogeneous strain tensor,  $\eta_i$ ; (3) local dimensionless displacements vectors,  $v_{ij}$ , defining the inhomogeneous strain;<sup>29,30</sup> (4) the pseudo-vector  $\omega_i$ , which is centered on Fe ions and represents oxygen octahedral tiltings (also known as antiferrodistortive (AFD) distortions) in unit cell  $i$ .<sup>31</sup> For instance,  $\omega_i = 0.1(\mathbf{x} + \mathbf{y} + \mathbf{z})$ , where  $\mathbf{x}$ ,  $\mathbf{y}$  and  $\mathbf{z}$  are the unit vectors along the three pseudo-cubic <001> directions, characterizes the tilting of the oxygen octahedron centered around the Fe site  $i$  by  $0.1\sqrt{3}$  radians about the pseudo-cubic [111] direction; and (5) the local magnetic moments  $m_i$  that are also centered on the Fe ions and whose magnitudes are equal to  $4\mu_B$ —as consistent with *ab initio* simulations<sup>32</sup> and experiments.<sup>33</sup> Note that we adopt a G-type antiferromagnetic structure here, as commonly found in BiFeO<sub>3</sub>

films.<sup>34</sup> We also concentrate on results at the temperature of 10 K for better statistics and to extract domain wall energies. Note also that the depth of the lattice potential (which is important to describe DW dynamic) should be well reproduced by the present model Hamiltonian since such model provides a very accurate Curie temperature for BFO bulks.<sup>26</sup>

### Relaxed domains

We practically consider two types of domain walls, namely  $109^\circ$  domains versus  $71^\circ$  domains, mainly because ref. <sup>11</sup> found that these domain walls are rather different in the sense that the  $71^\circ$  domains were measured to be much less conductive than the  $109^\circ$  domains for static or kHz conditions. A  $20 \times 10 \times 10$  periodic supercell is selected to represent the  $109^\circ$  domains. Figure 1a, b displays the snapshot of the dipolar pattern in a (010) and (001) plane, respectively, in this relaxed supercell (see three-dimensional (3D) plots in Supplement Materials). These figures indicate that our chosen supercell contains two ferroelectric domains that alternate along the pseudo-cubic [100] direction and that possess local dipoles being oriented along the pseudo-cubic [111] and [1-1-1] direction, respectively. The two ferroelectric domain walls are numerically found to be rather narrow and involve the 10th and 11th (100) Bi planes, and the 20th and (periodically repeating) 1st (100) Bi planes, respectively, as shown by red lines in Fig. 1a, b. Moreover, the tilting oxygen octahedral pattern adopts two different domains because of its known correlation with electric dipoles (that favor oxygen octahedra to tilt about the polarization axis),<sup>35,36</sup> as depicted in Fig. 1c, d: one for which the pseudo-

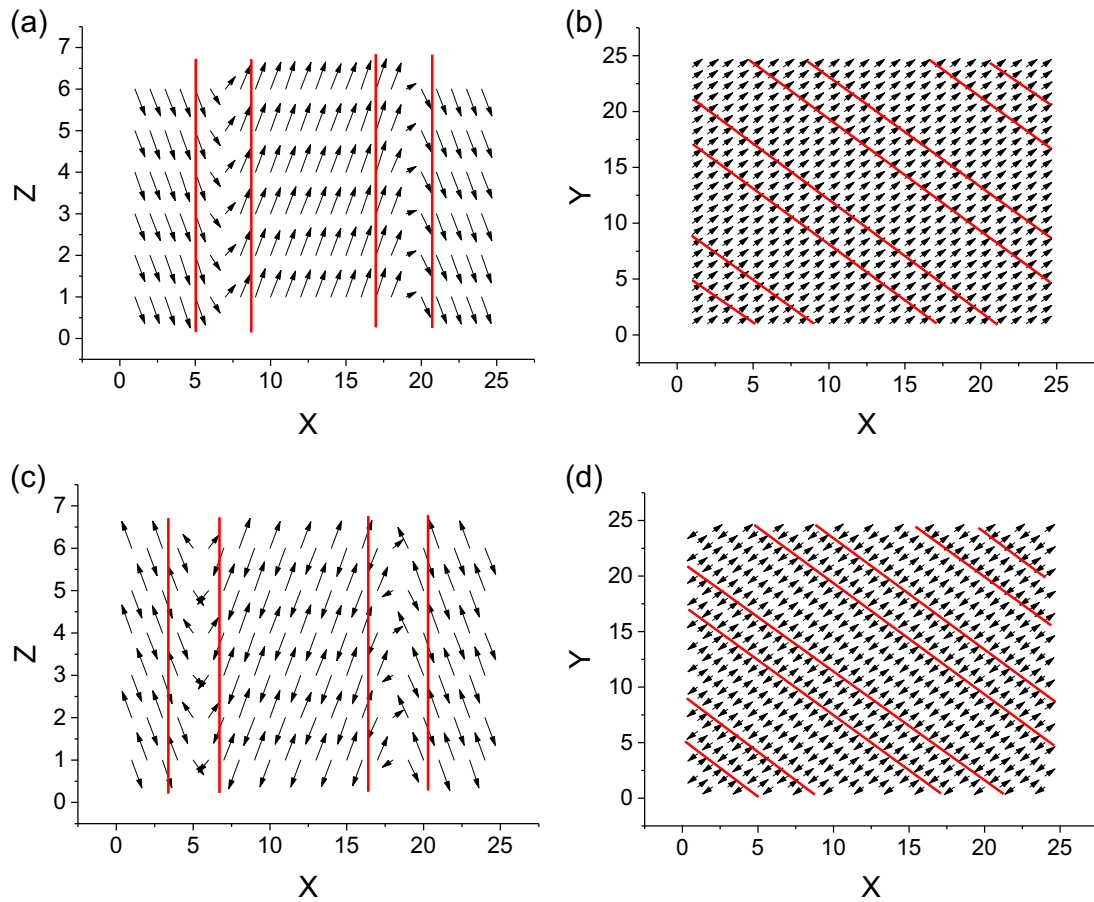


**Fig. 2** Same as Fig. 1 but for a  $71^\circ$  domain. Note the broader domain walls for the  $71^\circ$  domain with respect to the  $109^\circ$  domain case

vectors  $\omega_i$  are parallel or anti-parallel to the the  $[111]$  pseudo-cubic direction and another one for which  $\omega_i$  is oriented along  $[-111]$  or  $[1-1-1]$ . Figure 1c, d further indicates that the walls of these two AFD domains are narrow as well. The relaxed local dipole and tilting patterns depicted in Fig. 1 are similar to the lowest-in-energy  $109^\circ$  domains structure obtained from first principles in ref. 17. In particular, our computations and first-principles results both indicate that the dipoles located on the right side of the domain walls (e.g., layers 1 and 11 in our cases) have z-components of the dipoles that are smaller in magnitude than the other layers.

Regarding the  $71^\circ$  domains, we model them by choosing a  $24 \times 24 \times 6$  supercell that contains four different dipolar domains alternating along the  $[110]$  pseudo-cubic direction, as indicated in Fig. 2a, b (see 3D plots in Supplement Materials). Two of these domains have a polarization pointing along the pseudo-cubic  $[111]$  direction and are separated from each other by the other two domains for which the electric dipoles point along the pseudo-cubic  $[11-1]$  direction. The existence of these four dipolar domains, altogether with the coupling between local dipoles and oxygen octahedral tiltings, also led us to choose AFD patterns that are also forming four different domains: two for which  $\omega_i$  are parallel or anti-parallel to the the pseudo-cubic  $[111]$  direction versus two others for which the AFD pseudo-vector lies either parallel or antiparallel to the pseudo-cubic  $[11-1]$  direction. It is interesting to realize that the relaxation of our supercell leads to walls of the dipolar and antiferrodistortive patterns for the  $71^\circ$  domains that are wider than those of the  $109^\circ$  domains, with some layers adopting rather small z-components of their electric dipoles or AFD vectors (see the Bi-layers 6, 7, 19 and 20 in Fig. 2a having smaller z-component of the local modes, or the Fe-layers 5, 6, 18 and 19 in Fig. 2c having weaker oxygen octahedra tilting about

the z-axis). The local dipole and tilting patterns shown in Fig. 2 are also consistent with the first-principles work of ref. 17, and already point out to some differences (related to the width of the domain wall) between  $109^\circ$  and  $71^\circ$  domains—as also noted in a recent work.<sup>37</sup>

The domains' energies are numerically found to be equal to 73 and  $207 \text{ mJ/m}^2$  for our relaxed  $109^\circ$  and  $71^\circ$  domains, respectively. These predictions agree rather well with the corresponding ab initio values of 53 and  $62 \text{ mJ/m}^2$  for the  $109^\circ$  domains' energy versus 156 and  $167 \text{ mJ/m}^2$  for the  $71^\circ$  domains' energy,<sup>16,17</sup> especially when realizing that the precise value of the domain energy is rather sensitive to technical details (for instance, ref. 17 found that the  $71^\circ$  domains' energy can increase from 167 to  $197 \text{ mJ/m}^2$  using the same functional within density functional theory but with different ab initio codes). The fact that our predictions provide a smaller domains' energy for the  $109^\circ$  domains than the  $71^\circ$  domains is also consistent with the fact that the former domains are more often observed than the latter in BFO.<sup>38,39</sup>

#### Displacement currents

We now subject our two investigated domains to an external ac electric field having a 2.5 GHz frequency and that is oriented along the pseudo-cubic  $[111]$  direction, and allow these domains to relax under this field. This frequency of 2.5 GHz is chosen in order that it is small enough to be far away from resonant phonon frequencies (that are typically in the THz regime) while it is large enough to be treatable by our MD simulations (recall that a typical timescale for molecular dynamics is the picosecond). The magnitude of this electric field is chosen to be  $0.2\sqrt{3} \times 10^8 \text{ V/m}$ , because we

numerically found that it is weak enough to prevent the domain walls from moving from one plane to another. The MD simulations run over 1,000,000 steps, each lasting 0.5 fs. We calculate the averaged local mode in all the different Bi planes being parallel to the domain walls at each of these MD steps, and further average them over time intervals corresponding to 40,000 MD steps. The resulting quantity is denoted  $\langle u_l \rangle$ , where the  $l$  integer indexes the different aforementioned Bi planes. One can then determine the difference  $\Delta \langle u_l \rangle$  between  $\langle u_l \rangle$ 's of nearest time intervals (each including 40,000 MD steps). On the basis of this calculation, we estimate the displacement current in each layer  $\mathbf{j}_l = \Delta P_l / \Delta t = \frac{Z^* e \Delta \langle u_l \rangle}{a^2 40000 \times 0.5 \text{ fs}}$ , where  $Z^*$  is the Born effective charge associated with the local mode,  $e$  is the electronic charge and  $a$  is the 5-atom lattice constant.  $P_l$  is the polarization associated with layer  $l$ . Note that the displacement current should also theoretically involve  $\epsilon_0 \Delta E / \Delta t$ , where  $\epsilon_0$  is the permittivity of vacuum and  $E$  is the electric field. However, such latter contribution is numerically found to be about three orders of magnitude smaller than that stemming from the temporal change in polarization alone, and is thus neglected here.

Let us first concentrate on the longitudinal and transverse components of the  $j$ 's for the 109° domains, respectively, under the aforementioned ac electric field. The longitudinal components are denoted as  $j_{l, \text{long}}$  and correspond to current being along the pseudo-cubic [100] direction (that is along the direction of alternance of the 109° domains), while the selected transverse components, to be coined  $j_{l, \text{trans}}$ , are chosen to be along the pseudo-cubic [011] direction for these 109° domains. We numerically found that the time evolutions of both  $j_{l, \text{long}}$  and  $j_{l, \text{trans}}$  for any layer  $l$  are well described by the functions  $A_l \sin(2\pi\nu_{ac}t + \phi_l)$ , where  $\nu_{ac}$  is the 2.5 GHz frequency of the applied field and where  $A_l$  and  $\phi_l$  are shown in Fig. 3a, b, respectively, as a function of the layer index for both the longitudinal and transverse components of  $j_l$ . Figure 3a (see 3D plots in Supplement Materials) reveals that the Bi layers that exhibit the largest amplitude  $A_l$  of the displacement current in the 109° domains, both for the longitudinal and transverse components, are those located within the domain walls (e.g., layer 1 for  $j_{l, \text{long}}$  and layers 1 and 11 for  $j_{l, \text{trans}}$ ) while the layers being inside the domains respond much less to the ac electric field. The displacement current is thus rather selective of its location in BFO since it prefers to be enhanced in the domain walls rather than within the domains. One can also note that Fig. 3a further shows that the largest amplitude of  $j_{l, \text{long}}$  is at least two times smaller than the maximum  $A_l$  of  $j_{l, \text{trans}}$  in the 109° domains, therefore implying that it is more difficult to alter the component of the dipoles that is along (rather than perpendicular to) the normal of the domain walls. Figure 3b further indicates that  $\phi_l$  is rather close to  $\pi/2$  (in radians) for any layer  $l$  and for both the longitudinal and transverse components of the displacement current. As a result and once realizing that the applied ac electric field evolves in time as  $\sin(2\pi\nu_{ac}t)$ , both  $j_{l, \text{long}}$  and  $j_{l, \text{trans}}$  of the domains' layers follow more or less the time derivative of the electric field rather than the field itself. Such feature is consistent with the fact that the displacement current is related to the time derivative of the polarization (note that the small difference between the precise values of  $\phi_l$  shown in Fig. 3b and  $\pi/2$  is characteristic of a weak loss).

Let us now concentrate on the current displacements for the 71° domains for the same electric field of  $0.2\sqrt{3} \times 10^8$  V/m applied along the pseudo-cubic [111] direction. Its longitudinal components are now along the pseudo-cubic [110] direction (which is the direction of the alternance of the domains), while the chosen transverse components lie along the pseudo-cubic [001] direction (these transverse components correspond to the  $r$  subscript in ref. <sup>37</sup>). We numerically found that  $j_{l, \text{long}}$  and  $j_{l, \text{trans}}$  also behave as a function of time as  $A_l \sin(2\pi\nu_{ac}t + \phi_l)$  for any layer  $l$ , with the resulting  $A_l$  amplitude and  $\phi_l$  angle being displayed as a function of the layer index in Fig. 3c, d, respectively (see 3D plots in

Supplement Materials). The 71° domains exhibit some similarities with the previous case of 109° domains. For example, (1) the largest  $A_l$  amplitudes of the transverse components of the  $j$ 's in the 71° domains still occur for some domain walls' layers (e.g., layers 6 and 20 for both  $j_{l, \text{trans}}$  and  $j_{l, \text{long}}$ ); (2) the maximal amplitudes of the  $j_{l, \text{trans}}$  currents are much stronger, by a ratio of about 8 now, than those of  $j_{l, \text{long}}$ ; and (3) both  $j_{l, \text{trans}}$  and  $j_{l, \text{long}}$  continue to nearly follow the time derivative of the electric field (since, once again, the  $\phi_l$  angles of Fig. 3d are all close to  $\pi/2$  in radians). There are, however, also some differences with the aforementioned case of the 109° domains. For instance, there are more layers that adopt an enhancement of the amplitude of  $j_{l, \text{trans}}$  with respect to the value adopted by the transverse component of the displacement current at the heart of the domains in the 71° domains. As a matter of fact, layers 5, 6, 7, 8, 18, 19, 20 and 21 all have an  $A_l$  of  $j_{l, \text{trans}}$  that is at least four times as large as that of the internal layer 12, while only the layers 1 and 11 have an amplitude of  $j_{l, \text{trans}}$  that is stronger by a ratio of about 4 with respect to that of layers being deep inside domains (such as the layer 5) in the 109° domain case. Such difference originates from the fact that the 71° domain walls are broader as compared to the 109° domain walls, as seen by comparing Figs. 1a and 2a and as also emphasized in ref. <sup>37</sup>. One can also note that the  $A_l$ 's of the longitudinal components of the  $j$ 's are much smaller by at least a factor of 2 for any layer located at the domain walls in the 71° domains than in the 109° domains, which implies that it is typically more difficult to change the dipoles along the longitudinal direction at the 71° domain walls as compared to 109° domain walls.

#### Microscopic origins

Let us now try to find the effects responsible for striking features displayed in Fig. 3a, c, namely the facts that (1) the transverse displacement current is enhanced at the domain walls for both the 71° and 109° domains, and (2)  $j_{l, \text{trans}}$  is much stronger than  $j_{l, \text{long}}$  at these domain walls. For that, we decided to compute a physical quantity that can be taken to correspond to the individual dielectric response of layer  $l$  and which is defined (based on analogy with the formula known for the total dielectric response<sup>28,40,41</sup>) as :

$$\chi_{l, \alpha\beta}(\nu) = \frac{C_l}{T} \left[ \langle d_{l, \alpha}(t) d_{l, \beta}(t) \rangle + i2\pi\nu \int_0^\infty dt e^{i2\pi\nu t} \langle d_{l, \alpha}(t) d_{l, \beta}(0) \rangle \right], \quad (1)$$

where  $\nu$  is the frequency,  $\alpha$  and  $\beta$  define Cartesian components and  $T$  is temperature,  $d_{l, \alpha}(t)$  is the averaged local mode of layer  $l$  along the pseudocubic direction  $\alpha$  at time  $t$  and " $\langle \dots \rangle$ " indicates statistical average. Note that  $C_l$  is a normalization coefficient that is chosen such as, for the 71° and 109° domains, the largest peak of the imaginary part of  $\chi_l$  has a unity value in some domain wall layers.

Figure 4a, b reports the imaginary part of  $\chi_{l, \alpha\alpha}$  of layer 5 of the 109° domains as a function of frequency, with  $\alpha$  corresponding to the [100] longitudinal and [011] transverse direction, respectively. Such layer 5, that lies deep inside a domain (see Fig. 1a), has significant peaks in its individual dielectric response along the longitudinal direction at  $\approx 125, 201, 226$  and  $247 \text{ cm}^{-1}$  and also exhibits another strong peak near  $149 \text{ cm}^{-1}$  for the  $\chi_{l, \alpha\alpha}$  associated with the transverse direction. All these peaks are rather close to those located at 151, 176, 240 and  $263 \text{ cm}^{-1}$  in ref.<sup>28</sup>, and which correspond to phonon modes of  $E, A_1, E$  and  $A_1$  symmetry, respectively, in BFO *bulk*. In other words, one can posit that the layers lying inside domains in the 109° configuration adopt vibrations that are derived from those of the bulk. Such bulk-like modes can also be found when looking at Fig. 4c that displays the imaginary part of the individual dielectric response of layer 1 (which now lies inside the domain wall) of the 109° arrangement along the longitudinal direction. On the other hand, Fig. 4c further indicates the occurrence of a small and new peak at about

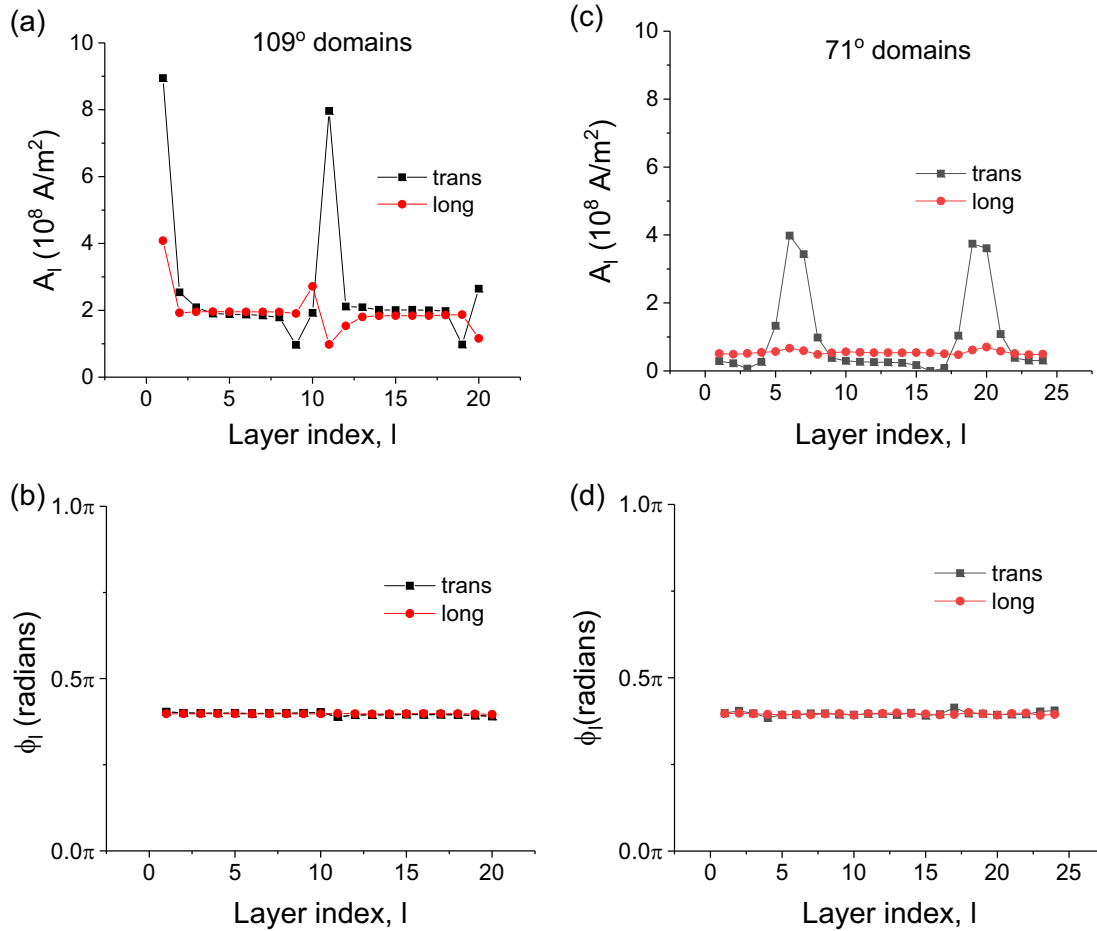


**Fig. 3** Quantities related to the time dependency of the calculated longitudinal and transverse displacement currents for the 109° and 71° domains of BFO. Panels **a, c** report the  $A_l$  amplitudes (see text), as a function of the index of the Bi layers being parallel to the domain wall, for the 109° and 71° domains, respectively. Panels **b, d** display the  $\phi_l$  angles (see text), as a function of this index too, for the 109° and 71° domains, respectively

$50 \text{ cm}^{-1}$  for this longitudinal response of layer 1 while Fig. 4d reveals that the imaginary part of the *transverse* dielectric response of this layer 1 possesses a strong peak close to  $\approx 50 \text{ cm}^{-1}$  too. The emergence of these low-frequency peaks indicate the formation of new soft vibrations that facilitate the change in electric dipoles at the walls of the 109° domains that, e.g., explains why  $A_l$  of layer 1 is large for both the longitudinal and transverse current displacements (see Fig. 3a). These soft vibrations can be thought to characterize dynamics of soliton-like<sup>42</sup> or kink-like objects<sup>43</sup> since such types of dynamics are usually associated with domain walls' motions. Note also that the fact that the  $\approx 50 \text{ cm}^{-1}$  peak of Fig. 4c, d has a larger intensity for the transverse direction than the longitudinal direction correlates with the enhancement of the amplitude of  $j_{l,trans}$  with respect to the amplitude of  $j_{l,long}$  for layer 1 (see Fig. 3a). Surprisingly, while the authors of ref. <sup>37</sup> also found bulk-like modes in 109° domains of BFO via the use of shell-model calculations, they did not predict the existence of any low-frequency optical mode there. We therefore wonder if their structure for the walls of 109° domains differs from our predicted one shown in Fig. 1 and thus also from that determined by ab initio calculations.<sup>17</sup>

Similar to the left column of Fig. 4, its right column also presents the imaginary part of  $\chi_{l,\alpha\alpha}$  as a function of frequency but for the 71° domains. More precisely, Fig. 4e, f shows the longitudinal and transverse individual dielectric response, respectively, of layer 12, which is located inside a domain of the 71° configuration. Moreover, Fig. 4g, h illustrates  $\chi_{l,\alpha\alpha}$  along the longitudinal [110]

and transverse [001] direction, respectively, in the layer 6 that belongs to a domain wall of the 71° domains (see Fig. 2a). Some bulk-like high-frequency peaks can be seen in Fig. 4e, f for the internal layer 12, such as a mode at  $203 \text{ cm}^{-1}$  for the longitudinal response and a mode with a frequency of  $138 \text{ cm}^{-1}$  for the transverse response. Interestingly, the strongest peaks of the imaginary part of the longitudinal individual response of the domain wall layer 6 also have high frequencies, namely ranging between  $\approx 125$  and  $\approx 200 \text{ cm}^{-1}$ . This feature correlates well with the facts that the amplitude of the longitudinal  $j_{l,long}$ : (1) is nearly the same in the layers belonging to domains or lying inside walls in the 71° configuration; (2) is also rather close to the  $A_l$  of the transverse  $j_{l,trans}$  of layers being inside domains (see Fig. 3c). In contrast, Fig. 4h reveals that the transverse part of  $\chi_{l,\alpha\alpha}$  for the domain wall layer 6 exhibits low-frequency vibrations, with two significant peaks at about  $24$  and  $35 \text{ cm}^{-1}$ . Such frequencies are even smaller than those about  $50 \text{ cm}^{-1}$  associated with the "kink-like" response of the domain wall of the 109° configuration displayed in Fig. 4d. They are in fact closer to the inhomogeneous phason-like vibration of about  $10 \text{ cm}^{-1}$  predicted to occur in ref. <sup>37</sup> for the 71° domains. Such low-frequency modes are also in line with the enhancement of the amplitude of  $j_{l,trans}$  depicted in Fig. 3c for the domain wall layers in the 71° domains, and were also proposed to explain the large  $zz$  component of the static dielectric response recently reported in ref. <sup>37</sup> for these domains (recall that our transverse component lies along the  $z$ -axis in the 71° domains).

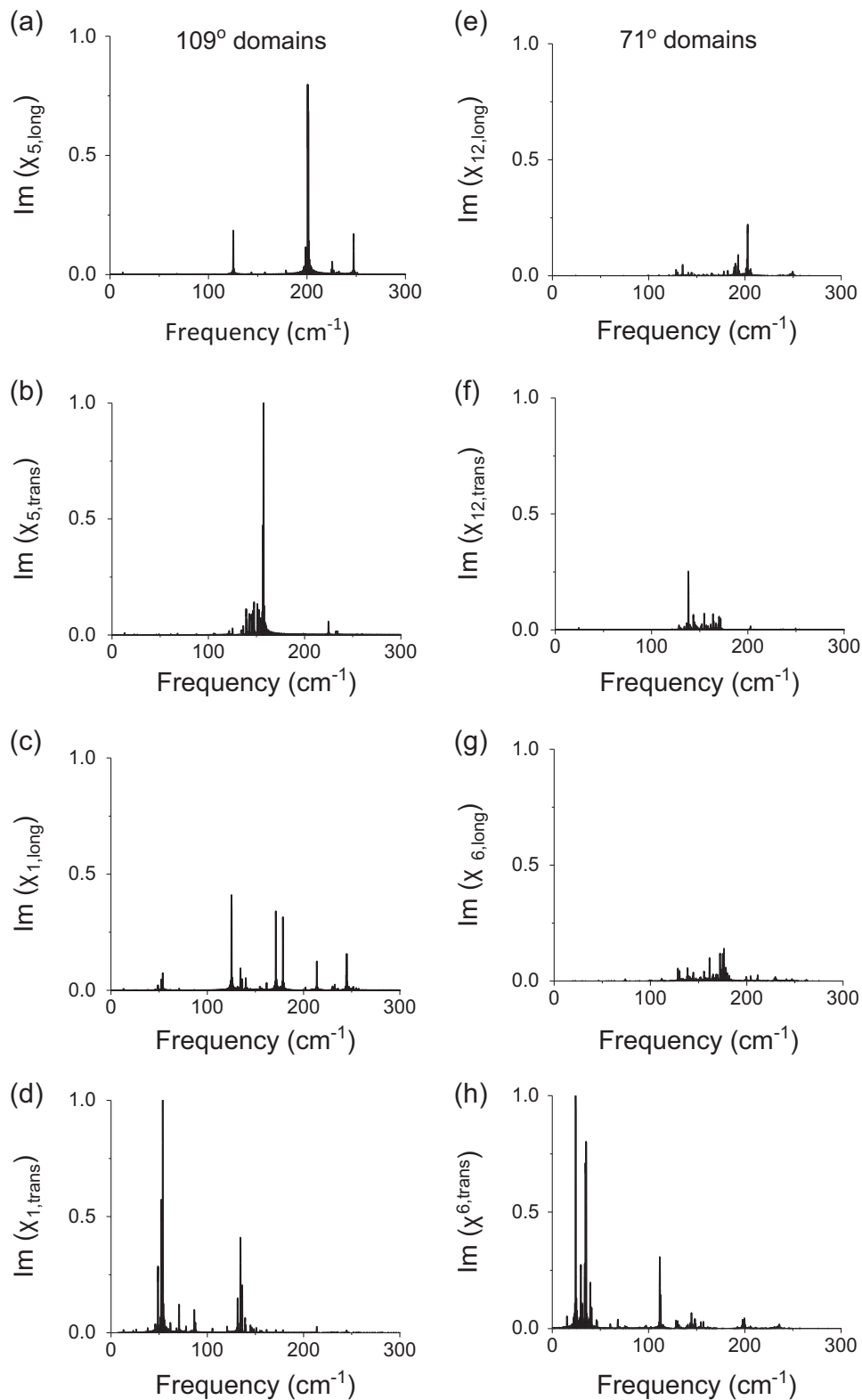


**Fig. 4** Imaginary part of the  $\chi_{i,aa}$  individual dielectric responses as a function of frequency for the  $109^\circ$  domains (**a–d**) and the  $71^\circ$  domains (**e–h**). Panels (**a, b**) correspond to the longitudinal and transverse direction, respectively, of the inside layer 5 of the  $109^\circ$  domains. Panels (**c, d**) are similar to (**a, b**), respectively, but for the domain wall layer 1. Panels (**e, f**) represent the longitudinal and transverse components, respectively, for the inside layer 12 of the  $71^\circ$  domains. Panels (**g, h**) are analogous to (**e, f**), respectively, but for the domain wall layer 6. Note that the magnitude of the response for both the  $109^\circ$  and the  $71^\circ$  domains is normalized such as the maximal peak has an intensity of 1

## DISCUSSION

Let us first indicate that atomistic simulations have the tendency to overestimate measured fields. For instance, ref. <sup>44</sup> reported an overestimation of a factor of about 20 in BiFeO<sub>3</sub>-related system. As a result, our simulated field of  $2\sqrt{3} \times 10^7$  V/m likely corresponds to an experimental field of about 1.5 MV/m. Note that such rescaled field of 1.5 MV/m is in fact smaller than the measured fields of 20–25 MV/m leading to a polarization switching in BFO<sup>45,46</sup> (note also that further simulations we performed do confirm that a theoretical dc field of  $2\sqrt{3} \times 10^7$  V/m is too small to switch the polarization). Moreover, we used an ac field of  $2\sqrt{3} \times 10^7$  of magnitude for two main reasons: (1) employing smaller fields leads to a response that is rather noisy and thus from which it is difficult to extract reliable data; and (2) employing larger fields (e.g.,  $\sqrt{3} \times 10^8$  V/m) was found to move the domain walls from one plane to another, rather than to have them to fluctuate around given, fixed planes.

Let us now start from the discussion of the significance of the soft modes located on DWs for the displacement current. Low-frequency modes were found when modeling BFO domains within shell model calculations<sup>37</sup> and when modeling domains and DWs' dynamics in an hexagonal manganate oxide<sup>20</sup> by employing a one-dimensional model Hamiltonian. In particular, Wu et al.<sup>20</sup> assumed that the electric current should also have a peak at the frequency of these modes, but did not provide arguments to explain why. In fact, such arguments can be provided based on the use of the displacement current. For that, let us take an electric field of the form  $E = E_0 \exp(i\omega t)$  and a resulting polarization of the form  $P = P_0 \exp(i\omega t)$ . The resulting current density is  $j = \frac{dP}{dt} = P_0 i \omega \exp(i\omega t)$ . Moreover, one can write the dielectric response as  $\chi = \frac{dP}{\epsilon_0 dE} = \frac{dP}{\epsilon_0 dt} \frac{dt}{dE} = \frac{P_0}{\epsilon_0 E_0}$ , where  $\epsilon_0$  is vacuum permittivity. As a result, a divergence in dielectric response at some resonant frequency will generate a divergence of  $P_0$ , which will in turn induce a divergence in the current density. Moreover, away from these resonances,  $\chi$  and  $P_0$  will be much smaller and  $j$  will then linearly increase with the  $\omega$  frequency from a constant finite value inherent to dc current.

Let us now compare the magnitude of the current density obtained in several experiments on different materials with our present calculations. For instance, the authors of ref. <sup>20</sup> used the scanning impedance microscope to measure the current near the DWs in some hexagonal manganate oxides. They found that the conductivity at 1 GHz is equal to 400 S/m, when the magnitude of the electric field under the tip is  $10^6$  V/m. The resulting current density is  $j = \sigma E = 4 \times 10^8$  A/m<sup>2</sup>. Interestingly, ref. <sup>19</sup> obtained a similar estimate of the current density in Pb(Zr,Ti)O<sub>3</sub> and BFO, as measured by scanning impedance microscope at 3 GHz.<sup>19</sup> Strikingly, Fig. 3a, b indicates that we predict (longitudinal) current density of the order of  $8\text{--}9 \times 10^8$  A/m<sup>2</sup> for 109° DWs and  $4 \times 10^8$  A/m<sup>2</sup> for 71° DWs for BFO at similar frequency (namely, 2.5 GHz). It thus appears that our results are comparable with the the experiments of refs. <sup>19,20</sup>. However, we should mention that the interpretations of the data in refs. <sup>19,20</sup> differ from ours. Indeed, the study of ref. <sup>20</sup> relates the microwave current to the DW' sliding mode, which corresponds to the acoustic vibrations of the DW, while the other study of ref. <sup>19</sup> relates this current to the charges emerging on the DW due to their roughening near point defects. In contrast, our calculations reveal the existence of a soft optical mode related to the DW vibrations in order to explain our predicted current density.

Let us now try to compare our results with the experiment of ref. <sup>11</sup> on BFO where an ac field was superimposed to a dc electric field.<sup>11</sup> In such case, both electronic and bound charges conductivity can in principle contribute to the measured current. Ref. <sup>11</sup> applies an ac field of the order of  $10^6$  V/m with frequency in the range of 200–350 kHz, and at the same time applies a dc field ranging between  $10^7$  and  $10^8$  V/m. Then, a current of 0.08–1 nA is

measured at 109° domains in ref. <sup>11</sup>. Similar orders of magnitude have been obtained in some other studies: for instance, ref. <sup>3</sup> observes a 9 nA current at 109° domains in ultra-high vacuum in a La-doped BFO thin film under an applied bias of roughly  $3.1 \times 10^7$  V/m. Let us thus estimate the current  $I$  induced in our studied 109° domain walls: our calculations predict a displacement current of  $8 \times 10^8$  A/m<sup>2</sup> for a applied electric field of  $\approx 3.5 \times 10^7$  V/m magnitude. Choosing a perpendicular area equal to  $1 \text{ nm} \times 10 \text{ nm}$ , where 1 nm roughly corresponds to the width of this domain wall (as consistent with Fig. 1a) and 10 nm is the length disturbed by the application of a tip in ref. <sup>11</sup>, provides an ac  $I$  current of 8 nA magnitude. Now, it is important to realize that, due to technical constraints, our simulation was performed with an applied frequency of 2.5 GHz. In contrast, a smaller 350 kHz frequency was applied in the experiment of ref. <sup>11</sup>. Remembering that the displacement current  $j_D \propto \frac{\partial P}{\partial t} \propto -i2\pi\nu P$  for a harmonic excitation of frequency  $\nu$ , we can estimate the displacement current at the frequency applied in ref. <sup>11</sup> to be  $j_D(350 \text{ kHz}) \approx j_D(2.5 \text{ GHz}) \times \frac{350 \text{ kHz}}{2.5 \text{ GHz}}$  which eventually results in a  $I$  current of 1.1 pA. This is roughly three to one orders of magnitude smaller than values measured in different experiments for similar electric field amplitude.<sup>2–4,11</sup> As a result, low-frequency conductivity is most likely associated with electronic features such as possible band-gap reduction,<sup>3</sup> Schottky barrier lowering by defects,<sup>47,48</sup> increased concentration of free carriers at the domain wall caused by flexoelectric and deformation potential effects of curved domain walls<sup>49</sup> or defect accumulation.<sup>2,3</sup> In other words, ionic contributions should be negligible in the frequency range investigated by those works.

However, although bound charges conductivity may not be important at low frequencies, they become sizable contributions at larger ones, according to the presently reported simulations. As a matter of fact and as discussed in the previous paragraph, the estimated  $I$  current of 8 nA at 2.5 GHz is of the same order of magnitude or even larger than the measured dc currents reported in the literature for similar applied electric fields.<sup>2,4,11,48</sup> This opens the way towards the design of fast nanoscale electronic circuits operating in the GHz or THz range, and in which currents would be confined in the domain wall. To that end, the existence of resonance modes intrinsic to the domain wall, as discussed previously, could be particularly helpful. We also note that the sizable contribution of displacement currents at large frequencies (or small time scales) can possibly explain the large transient enhancement of the current observed upon application of an electric field pulse of magnitude  $0.4 \times 10^7$  V/m in 109° domain walls (see Fig. 2b of ref. <sup>11</sup>). Note also that we conducted simulations with larger electric fields ( $\sqrt{3} \times 10^8$  and  $5\sqrt{3} \times 10^8$  V/m for 71° and 109° domains respectively), and found (not shown here) that temporal jumps in the displacement current appeared due to the *motion* of the domain wall. These transient currents are one order of magnitude larger than those reported here in Fig. 3 for smaller electric fields, and may very well participate to the transient current peaks observed in ref. <sup>11</sup> too.

It is also worthwhile to indicate that our calculations corresponding to Fig. 3 indicate that the 109° and 71° domain walls should produce roughly the same amount of  $I$  current. Indeed, comparing Fig. 3a, c indicates that the maximal  $A_j$ 's for the transverse components of the current displacements in the domain walls are smaller by a factor of around 2 in the 71° domains with respect to those of the 109° domains. Such decrease of the maximal amplitude of  $j_{I,trans}$  by a factor of 2, accompanied by an enhancement of the domain wall width by about a factor of 2 (compare Figs. 1a and 2a), when going from the 109° to 71° domain walls, lead to an estimated maximal transverse  $I$  current being in fact similar in these two domain walls (provided the AFM tip is larger than the width of both domain walls). As a result, the transverse dynamical conductivity should be of the same order of magnitude in these two types of domains. This prediction contrasts with experiments demonstrating much larger (dc-like)

conductivity of the 109° domains with respect to the 71° domains<sup>50</sup> or even no conductivity at all in these latter domains.<sup>2</sup> Note, however, that there exist contradictory reports of the conduction state of the 71° domain wall that have, for instance, been found in ref. <sup>4</sup>, further pointing at a possible important contribution of the defect accumulation at neutral domain wall to conductivity<sup>18,51</sup> (note that the presence of defects may impede the observation of the intrinsic displacement current<sup>19</sup>). On the other hand, we predict here that enhanced displacement current can intrinsically exist in both 109° and 71° domains in the GHz and above regimes as no defects or interfaces were considered in our calculations. In other words, this intrinsic effect should be rather robust against material synthesis and processing.

In summary, we conducted atomistic simulations to investigate intrinsic displacement currents in neutral 109° and 71° domains of BFO in the GHz range. It is predicted that such displacement currents, especially their transverse component, are rather significant at the domain walls, as a result of localized low-frequency optical vibrations. In particular, the corresponding intrinsic polarization-originating *I* current can be as large as, or even larger than, the likely electronic-driven and extrinsic current reported for static or kHz conditions. Such finding may open the door for the realization of new devices operating in the GHz or THz range.

## METHODS

Here, we use the effective Hamiltonian scheme that has been documented in detail in ref. <sup>26</sup>. Technically, such scheme is presently implemented in a Molecular Dynamics technique (see refs. <sup>27,28</sup> for more details).

## Data availability

The authors declare that all data supporting the findings of this study are available within the paper and its supplementary information file.

## ACKNOWLEDGEMENTS

This work is supported by ONR Grants No. N00014-12-1-1034 and N00014-17-1-2818. L.B. also thanks the DARPA Grant No. HR0011727183-D18AP00010. Y.Y. is thankful for the discussion with Dr. Bin Xu. S.P. appreciates support of RMES 3.1649.2017/4.6 and RFBR 18-52-00029 Bel<sub>a</sub>.

## AUTHOR CONTRIBUTIONS

Y.Y. proposed the topic of the study, and implemented the subroutine to compute displacement current. S.P. and Y.Y. performed the effective Hamiltonian simulations, and analyzed the results along with C.P. and L.B. Different parts of the original version of the manuscript were written by S.P., C.P. and L.B., which was then modified due to the feedback and suggestions of all authors. Y.Y. and S.P. contributed equally.

## ADDITIONAL INFORMATION

**Supplementary information** accompanies the paper on the *npj Computational Materials* website (<https://doi.org/10.1038/s41524-018-0066-y>).

**Competing interests:** The authors declare no competing interests.

**Publisher's note:** Springer Nature remains neutral with regard to jurisdictional claims in published maps and institutional affiliations.

## REFERENCES

- Catalan, G., Seidel, J., Ramesh, R. & Scott, J. F. Domain wall nanoelectronics. *Rev. Mod. Phys.* **84**, 119 (2012).
- Seidel, J. et al. Conduction at domain walls in oxide multiferroics. *Nat. Mater.* **8**, 229–234 (2009).
- Seidel, J. et al. Domain wall conductivity in La-doped BiFeO<sub>3</sub>. *Phys. Rev. Lett.* **105**, 197603 (2010).
- Farokhipoor, S. & Noheda, B. Conduction through 71° domain walls in BiFeO<sub>3</sub> thin films. *Phys. Rev. Lett.* **107**, 127601 (2011).
- Guyonnet, J., Gaponenko, I., Gariglio, S. & Paruch, P. Conduction at domain walls in insulating Pb(Zr<sub>0.2</sub>Ti<sub>0.8</sub>)O<sub>3</sub> thin films. *Adv. Mater.* **23**, 5377–5382 (2011).
- Aird, A. & Salje, E. K. H. Sheet superconductivity in twin walls: experimental evidence of WO<sub>3-x</sub>. *J. Phys. Condens. Matter.* **10**, L377–L380 (1998).
- Farokhipoor, S. et al. Artificial chemical and magnetic structure at the domain walls of an epitaxial oxide. *Nature* **515**, 379–383 (2014).
- Parkin, S. S. P., Hayashi, M. & Thomas, L. Magnetic domain-wall racetrack memory. *Science* **320**, 190–194 (2008).
- Chu, Y. H. et al. Nanoscale control of domain architectures in BiFeO<sub>3</sub> thin films. *Nano. Lett.* **9**, 1726–1730 (2009).
- Balke, N. et al. Deterministic control of ferroelastic switching in multiferroic materials. *Nat. Nanotechnol.* **4**, 868–875 (2009).
- Maksymovych, P. et al. Dynamic conductivity of ferroelectric domain walls in BiFeO<sub>3</sub>. *Nano. Lett.* **11**, 1906–1912 (2011).
- Vasudevan, R. K. et al. Domain wall conduction and polarization-mediated transport in ferroelectrics. *Adv. Funct. Mater.* **23**, 2592–2616 (2013).
- Kim, K.-E. et al. Electric control of straight stripe conductive mixed-phase nanostructures in La-doped BiFeO<sub>3</sub>. *NPG Asia Mater.* **6**, e81 (2014).
- Morozovska, A. N., Vasudevan, R. K., Maksymovych, P., Kalinin, S. V. & Eliseev, E. A. Anisotropic conductivity of uncharged domain walls in BiFeO<sub>3</sub>. *Phys. Rev. B* **86**, 085315 (2012).
- Lubk, A., Gemming, S. & Spaldin, N. A. First-principles study of ferroelectric domain walls in multiferroic bismuth ferrite. *Phys. Rev. B* **80**, 104110 (2009).
- Ren, W. et al. Ferroelectric domains in multiferroic BiFeO<sub>3</sub> films under epitaxial strains. *Phys. Rev. Lett.* **110**, 187601 (2013).
- Diéguez, O., Aguado-Puente, P., Junquera, J. & Íñiguez, J. Domain walls in a perovskite oxide with two primary structural order parameters: first-principles study of BiFeO<sub>3</sub>. *Phys. Rev. B* **87**, 024102 (2013).
- Rojac, T. et al. Domain-wall conduction in ferroelectric BiFeO<sub>3</sub> controlled by accumulation of charged defects. *Nat. Mat.* **16**, 322 (2017).
- Tselev, A. et al. Microwave a.c. conductivity of domain walls in ferroelectric thin films. *Nat. Commun.* **7**, 11630 (2016).
- Wu, X. et al. Low-energy structural dynamics of ferroelectric domain walls in hexagonal rare-earth manganites. *Sci. Adv.* **3**, e1602371 (2017).
- Dzyaloshinskii I. E., I. E. & Mills, D. L. Intrinsic paramagnetism of ferroelectrics. *Philos. Mag.* **89**, 22–24 (2009). 2079–2082.
- Albrecht, D. et al. Ferromagnetism in multiferroic BiFeO<sub>3</sub> films: a first-principles-based study. *Phys. Rev. B* **81**, 140401 (2010).
- Kornev, I. A., Lisenkov, S., Haumont, R., Dkhil, B. & Bellaiche, L. Finite-temperature properties of multiferroic BiFeO<sub>3</sub>. *Phys. Rev. Lett.* **99**, 227602 (2007).
- Lisenkov, S., Kornev, I. A. & Bellaiche, L. Properties of multiferroic BiFeO<sub>3</sub> under high magnetic fields from first principles. *Phys. Rev. B* **79**, 012101 (2009).
- Lisenkov, S., Kornev, I. A. & Bellaiche, L. Properties of multiferroic BiFeO<sub>3</sub> under high magnetic fields from first principle. *Phys. Rev. B* **79**, 219902 (2009).
- Prosandeev, S., Wang, D., Ren, W., Íñiguez, J. & Bellaiche, L. Novel nanoscale twinned phases in perovskite oxides. *Adv. Funct. Mater.* **23**, 234–240 (2013).
- Laguta, V. V. et al. Room-temperature paramagnetolectric effect in magneto-electric multiferroics Pb(Fe<sub>1/2</sub>Nb<sub>1/2</sub>)O<sub>3</sub> and its solid solution with PbTiO<sub>3</sub>. *J. Mater. Sci.* **51**, 5330–5342 (2016).
- Wang, D., Weerasinghe, J. & Bellaiche, L. Atomistic molecular dynamic simulations of multiferroics. *Phys. Rev. Lett.* **109**, 067203 (2012).
- Zhong, W., Vanderbilt, D. & Rabe, K. M. Phase transitions in BaTiO<sub>3</sub> from first principles. *Phys. Rev. Lett.* **73**, 1861 (1994).
- Zhong, W., Vanderbilt, D. & Rabe, K. M. First-principles theory of ferroelectric phase transitions for perovskites: the case of BaTiO<sub>3</sub>. *Phys. Rev. B* **52**, 6301 (1995).
- Kornev, I. A., Bellaiche, L., Janolin, P. E., Dkhil, B. & Suard, E. Phase diagram of Pb(Zr,Ti)O<sub>3</sub> solid solutions from first principles. *Phys. Rev. Lett.* **97**, 157601 (2006).
- Neaton, J. B., Ederer, C., Waghmare, U. V., Spaldin, N. A. & Rabe, K. M. First-principles study of spontaneous polarization in multiferroic BiFeO<sub>3</sub>. *Phys. Rev. B* **71**, 014113 (2005).
- Fischer, P., Polomska, M., Sosnowska, I. & Szymanski, M. Temperature dependence of the crystal and magnetic structures of BiFeO<sub>3</sub>. *J. Phys. C* **13**, 1931–1940 (1980).
- Sando, D. et al. Crafting the magnonic and spintronic response of BiFeO<sub>3</sub> films by epitaxial strain. *Nat. Mater.* **12**, 641–646 (2013).
- Xu, B. et al. Hybrid improper ferroelectricity in multiferroic superlattices: finite-temperature properties and electric-field-driven switching of polarization and magnetization. *Adv. Funct. Mater.* **25**, 3626–3633 (2015).
- Kornev, I. A. & Bellaiche, L. Nature of the ferroelectric phase transition in multiferroic BiFeO<sub>3</sub> from first principles. *Phys. Rev. B* **79**, 100105(R) (2009).
- Hlinka, J., Paściak, M., Körbel, S. & Marton, P. Terahertz-range polar modes in domain-engineered BiFeO<sub>3</sub>. *Phys. Rev. Lett.* **119**, 057604 (2017).
- Borodavka, F., Pokorny, J. & Hlinka, J. Combined piezoresponse force microscopy and Raman scattering investigation of domain boundaries in BiFeO<sub>3</sub> ceramics. *Phase Transit.* **89**, 746–751 (2016).

39. Sander, A., Christl, M., Chiang, C.-T., Alexe, M. & Widdra, W. Domain imaging on multiferroic BiFeO<sub>3</sub> (001) by linear and circular dichroism in threshold photoemission. *J. Appl. Phys.* **118**, 224102 (2015).
40. Ponomareva, I., Bellaiche, L., Ostapchuk, T., Hlinka, J. & Petzelt, J. Terahertz dielectric response of cubic BaTiO<sub>3</sub>. *Phys. Rev. B* **77**, 012102 (2008).
41. Caillol, J., Levesque, D. & Weis, J. Theoretical calculation of ionic solution properties. *J. Chem. Phys.* **85**, 6645–6657 (1986).
42. Dodd, R. K., Eilbeck, J. C., Gibbon, J. D. & Morris, H. C. *Solitons and Nonlinear Wave Equations* (Academic Press INC, London, 1982).
43. Buijnsters, F. J., Fasolino, A. & Katsnelson, M. I. Motion of domain walls and the dynamics of kinks in the magnetic Peierls potential. *Phys. Rev. Lett.* **113**, 217202 (2014).
44. Xu, B., Íñiguez, J. & Bellaiche, L. Designing lead-free antiferroelectrics for energy storage. *Nat. Commun.* **8**, 15682 (2017).
45. Ryu, S., Son, J. Y., Shin, Y.-H., Jang, H.-M. & Scott, J. F. Polarization switching characteristics of thin BiFeO<sub>3</sub> films epitaxially grown on PtMgO at a low temperature. *Appl. Phys. Lett.* **95**, 242902 (2009).
46. Baek, S. H. & Eom, C. B. Reliable polarization switching of BiFeO<sub>3</sub>. *Philos. Trans. R. Soc. A* **370**, 4872 (2012).
47. Farokhipoor, S. & Noheda, B. Local conductivity and the role of vacancies around twin walls of (001)-BiFeO<sub>3</sub> thin films. *J. Appl. Phys.* **112**, 52003 (2012).
48. Stolichnov, I. et al. Persistent conductive footprints of 109° domain walls in bismuth ferrite films. *Appl. Phys. Lett.* **104**, 132902 (2014).
49. Morozovska, A. N. Domain wall conduction in ferroelectrics. *Ferroelectrics* **438**, 3–19 (2012).
50. Vasudevan, R. K. et al. Domain wall geometry controls conduction in ferroelectrics. *Nano. Lett.* **12**, 5524–5531 (2012).
51. Paillard, C., Geneste, G., Bellaiche, L. & Dkhil, B. Vacancies and holes in bulk and at 180° domain walls in lead titanate. *J. Phys. Condens. Matter* **29**, 485707 (2017).



**Open Access** This article is licensed under a Creative Commons Attribution 4.0 International License, which permits use, sharing, adaptation, distribution and reproduction in any medium or format, as long as you give appropriate credit to the original author(s) and the source, provide a link to the Creative Commons license, and indicate if changes were made. The images or other third party material in this article are included in the article's Creative Commons license, unless indicated otherwise in a credit line to the material. If material is not included in the article's Creative Commons license and your intended use is not permitted by statutory regulation or exceeds the permitted use, you will need to obtain permission directly from the copyright holder. To view a copy of this license, visit <http://creativecommons.org/licenses/by/4.0/>.

© The Author(s) 2018